JTTEE5 20:145–153
DOI: 10.1007/s11666-010-9583-z
1059-9630/$19.00 © ASM International

Preparation of Nanocomposite GDC/LSCF Cathode Material for IT-SOFC by Induction Plasma Spraying

Yan Shen, Veronica Alexandra B. Almeida, and François Gitzhofer

(Submitted May 1, 2010; in revised form October 10, 2010)

Homogeneous mixtures of $Ce_{0.8}Gd_{0.2}O_{1.9}$ (GDC) and $La_{0.6}Sr_{0.4}Co_{0.2}Fe_{0.8}O_3$ (LSCF) nanopowders were successfully synthesized using induction plasma by axial injection of a solution. The resulting nanocomposite powders consisted of two kinds of nanopowders with different mass ratio of GDC/LSCF, such as 3/7 and 6/4. The morphological features, crystallinity, and the phases of the synthesized powders were characterized by scanning electron microscopy (SEM), transmission electron microscopy (TEM), local energy-dispersive x-ray spectroscopy (EDS) analysis, and x-ray diffraction (XRD). The nanopowders are almost globular in shape with a diameter smaller than 100 nm and their BET specific areas are around 20 $m^2\ g^{-1}$. The GDC and LSCF phases are well distributed in the nanopowders. In addition, suspensions, made with the as-synthesized composite nanopowders and ethanol, were used to deposit cathode coatings using suspension plasma spray (SPS). Micro-nanostructures of the coatings are discussed. The coatings are homogeneous and porous (51% porosity) with cauliflower structures.

Keywords gadolinium doped ceria (GDC), induction plasma, intermediate temperature solid oxide fuel cell (IT-SOFC), lanthanum strontium cobalt iron oxide (LSCF), nanocomposite powder, solution plasma spray (SolPS), suspension plasma spray (SPS)

1. Introduction

On the path to commercialize reliable solid oxide fuel cells (SOFCs), the intermediate temperature solid oxide fuel cells (IT-SOFCs) are getting increased attention. When the operating temperature gets lower, the cell lifetime can be prolonged because of the potentially improved long-term stability of the material. Besides, the system costs can be reduced using lower-cost materials. However, when the operating temperature is decreased, the interfacial polarization resistance of the cathode dramatically increases leading to a high cell voltage loss, which can be as high as 65% of the total voltage loss in the IT-SOFCs (Ref 1). To overcome this problem, the polarization resistance must be lowered at intermediate temperature. Recently, research on cathodes has focused on two aspects: (a) to develop materials with both high ionic and electronic conductivities, by adding a second phase with high ionic conductivity into the original cathode material; (b) based on the triple phase boundary (TPB) theory, to propose a novel microstructure with enlarged TPB, using nanostructured and graded composite cathodes.

Lanthanum strontium cobalt iron oxide, $La_xSr_{1-x}Co_yFe_{1-y}O_{3-\delta}$ is a mixed ionic-electronic conductor with significant electronic conductivity, as $La_{0.6}Sr_{0.4}Co_{0.2}Fe_{0.8}O_{3-\delta}$ (LSCF) has a high electrical conductivity of 275 S cm^{-1} at 600 °C (Ref 2). However, the ionic conductivity of $La_xSr_{1-x}Co_yFe_{1-y}O_3$ drops rapidly with temperature. Hence, in order to enhance the ionic conductivity, gadolinium-doped cerium is added to $La_xSr_{1-x}Co_yFe_{1-y}O_{3-\delta}$. As reported by Dusastre and Kilner (Ref 3), the polarization resistance of cathodes of LSCF with 30 wt.% $Ce_{0.9}Gd_{0.1}O_{2-\delta}$ was decreased by four times. Murray et al. (Ref 4) indicated the optimal cathode was LSCF with 50 wt.% $Ce_{0.8}Gd_{0.2}O_{1.9}$ (GDC), which had a polarization resistance about 10 times smaller. Leng et al. (Ref 5) found that a polarization resistance of 0.17 Ω cm^2, seven times lower than that of the pure LSCF cathode, was obtained at 600 °C when the GDC concentration was 60 wt.%. In this study, therefore, two kinds of nanocomposite powders used for IT-SOFC cathode material were made. One was LSCF mixed with 30 wt.% GDC, and the other was mixed with 60 wt.% GDC. Both these nanopowders were synthesized by induction solution plasma spray (SolPS) using mixed metal nitrate solutions

This article is an invited paper selected from presentations at the 2010 International Thermal Spray Conference and has been expanded from the original presentation. It is simultaneously published in *Thermal Spray: Global Solutions for Future Applications, Proceedings of the 2010 International Thermal Spray Conference*, Singapore, May 3-5, 2010, Basil R. Marple, Arvind Agarwal, Margaret M. Hyland, Yuk-Chiu Lau, Chang-Jiu Li, Rogerio S. Lima, and Ghislain Montavon, Ed., ASM International, Materials Park, OH, 2011.

Yan Shen, Veronica Alexandra B. Almeida, and **François Gitzhofer**, Chemical and Biotechnical Engineering Department, Energy, Plasma and Electrochemistry Research Centre (CREPE), Université de Sherbrooke, Sherbrooke, QC J1K 2R1, Canada. Contact e-mails: Francois.Gitzhofer@USherbrooke.ca and Yan.Shen@Usherbrooke.ca.

as the precursors. Although there were several previous studies on synthesizing cathode materials by induction plasma (Ref 6, 7), no published research is available on the synthesis of the nanocomposite powders using induction plasma technology. This method not only promises nanosized particle powders with the exact compositions but also provides an efficient way to synthesize the uniformly distributed composite nanopowders avoiding long sintering time and contaminations associated with any mechanical mixing process.

In this study, the composite nanopowder was also used in a next step to produce cathode coatings by suspension plasma spray (SPS), a method which eases the fabrication of nanostructured coatings and was invented in the middle of the 1990s by Université de Sherbrooke (Ref 7, 8). Compared to the various techniques which have been employed to produce graded cathodes: screen printing, slurry spraying and coating, spray painting, electrostatic spray deposition, combustion chemical vapour deposition, etc. (Ref 9-13), the suspension induction plasma spray technique provides a more cost effective way to produce the coatings without long-time sintering. Besides, it is particularly adapted to produce functionally graded coatings by alternating the injected precursors. In this article, the nanocomposite powder properties are presented and followed by some preliminary results of plasma-sprayed composite cathode coatings for IT-SOFC.

2. Experiments

2.1 Powder Synthesis Method

2.1.1 Solution Precursor Preparation. The nanocomposite powders, GDC/LSCF with a ratio of GDC to LSCF 60:40 wt.% (GDC6/LSCF4) and GDC/LSCF with a 30:70 wt.% ratio (GDC3/LSCF7), were synthesized by induction SolPS technique from corresponding metal nitrate solutions.

For the LSCF metal nitrate solution, nitrates such as $La(NO_3)_3{\cdot}6H_2O$ (99.9%, Alfa Aesar, Wardhill, MA), $Sr(NO_3)_2$ (98%, Alfa Aesar, Wardhill, MA), $Co(NO_3)_2{\cdot}6H_2O$ (97.9% min, Alfa Aesar, Wardhill, MA), and $Fe(NO_3)_3{\cdot}9H_2O$ (98+%, Alfa Aesar, Wardhill, MA), were stoichiometrically mixed and dissolved into distilled water to obtain a concentration of 1.1 M solution. For the GDC metal nitrate solution, $Gd(NO_3)_3{\cdot}6H_2O$ (99.9%, Aldrich, Milwaukee, WI) and $Ce(NO_3)_3{\cdot}6H_2O$ (99%, Aldrich, Milwaukee, WI) were added to the LSCF nitrate solution according to the theoretical mass ratios of GDC to LSCF in GDC6/LSCF4 and GDC3/LSCF7. Finally, Glycine (98.5%, Alfa Aesar, Wardhill, MA) was added to the solution at a concentration of 1.45 M.

2.1.2 SolPS of Cathode Nanopowders. The induction plasma synthesis technique via solution plasma spraying was used to synthesize nanopowders. Figure 1(a) presents the induction plasma powder synthesis system. The plasma was generated by a Tekna Plasma Systems (Sherbrooke, Québec, Canada) PL50 torch, Fig. 1(b). The torch was connected to a 3 MHz LEPEL HF power generator. The

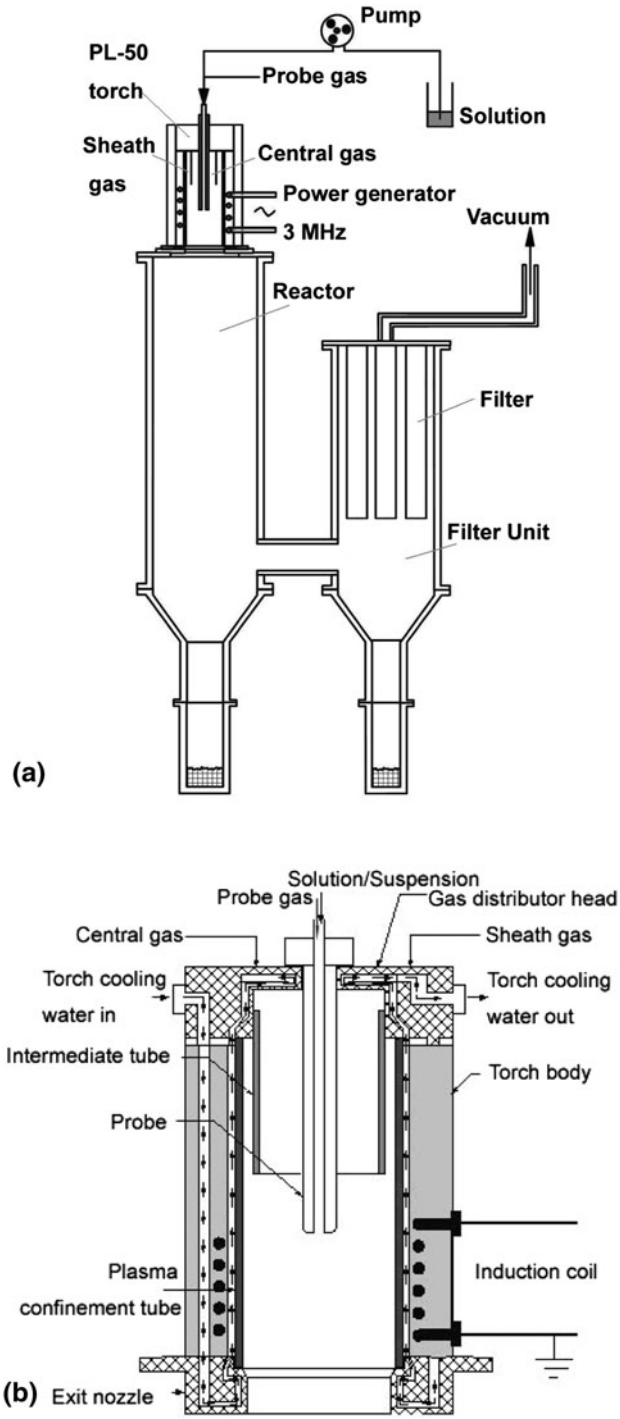

Fig. 1 (a) Nanopowder synthesis system and (b) induction plasma torch (Ref 14)

plasma plume was formed inside the torch by partially ionizing the central gas (Argon) and the sheath gas (Oxygen). The intermediate tube, made of quartz, was used to separate the sheath gas from the central gas. A 50-mm diameter ceramic tube was used as the plasma confinement tube followed by an exit nozzle with a diameter of 45 mm. The system also contained a reactor

and filter unit, which included porous metal filters. Both the reactor and filter unit were continually water-cooled with a double wall system during the synthesis.

When the plasma became stable under required experimental conditions, the nitrate solution was injected into its axis by a peristaltic pump and directly atomized by a centrally located probe. After some chemical and physical reactions, the nanopowders were adsorbed on the inner-faces of both of the reactor and the filter unit as well as on the surface of the filters. During the powder synthesis, the solution feeding rate was kept at 5 mL min^{-1}. All the plasma operating conditions are presented in Table 1.

2.2 Cathode Deposition Using SPS

2.2.1 Suspension Precursor Preparation. The as-synthesized SolPS GDC6/LSCF4 nanopowders were used to deposit cathodes by the SPS process using an induction plasma. Ethanol was used as the solvent and 12 wt.% of GDC6/LSCF4 nanopowders were loaded into it. Before deposition, the suspension was treated with an ultrasonic processor for 10 min in order to break the agglomerated particles. During the SPS deposition, a magnetic stirrer was used to prevent the suspension from settling.

2.2.2 SPS Experimental Set-Up and Procedures. The cathode coating was deposited by the suspension spraying method with previously synthesized GDC6/LSCF4 nanopowder. In this process, the induction plasma system was the same as described in section 2.1.2. However, the nanopowder synthesis reactor and the filter unit were replaced by a large vacuum chamber (Fig. 2), where the deposition was carried out. A programmable sting carried the sample holder and moved it back and forth under the plasma plume. The offset, translating distance, moving velocity and the numbers of loops of the sting were able to be altered. In addition, the distance between the sample holder and the torch nozzle could be adjusted as well to control the microstructure and morphology of the deposited layer.

The substrate was made of a porous hastelloy support with four successive layers deposited on top of it. The porous hastelloy support (SIKA-Hastelloy X) with 1-μm pore size was purchased from GKN Sinter Metals Filters Company (Naperville, IL, USA). Those successive four layers were deposited by suspensions of 8 wt.% NiO-Fe_2O_3, 3 wt.% GDC, 8 wt.% LSGM8282 ($La_{0.8}Sr_{0.2}Ga_{0.8}Mg_{0.2}O$) and 8 wt.% LSGFM ($La_{0.8}Sr_{0.2}Ga_{0.7}Fe_{0.2}Mg_{0.1}O_3$), respectively, using induction plasma spray technology. The substrates passed through the plasma plume 30 times to build up cathode coatings. Optimized plasma parameters applied for the SPS deposition are presented in Table 2 and the suspension feeding rate was 15 mL min^{-1}.

2.3 Characterization and Analysis

The structural analyses of the nanopowders were conducted by x-ray diffraction (XRD) using a Philips X'Pert Pro MPD x-ray diffractometer (Eindhoven, Netherlands). The morphologies of the nanopowders were observed using a Hitachi S4700 Field Emission Scanning Electron Microscope (FE-SEM) (Tokyo, Japan) and Hitachi 7500 and Jeol JEM-2100F Transmission Electron Microscopes (Tokyo, Japan) (TEM). The BET specific areas of the powders were determined using a Quantachrome Autosorb-1 automated gas sorption system with Nitrogen (Quantachrome Corporation, FL, USA). Energy-dispersive x-ray spectroscopy (EDS) composition measurement was done locally with a 2-nm resolution on the nanocomposite powders using the Jeol JEM-2100F to locally measure the composition of the nanopowders.

Morphologies and microstructures of the deposited cathode coatings were examined by a Hitachi VPSEM S3000N SEM (Tokyo, Japan) and the higher resolution FE-SEM. The porosity of the coating was determined by image analysis of five pictures taken at different places on polished sections of the sample at 20 kV, 5.0 kX magnification. Using the image analysis software SigmaScan Pro from Systat Software Inc. (San Jose, CA, USA), a threshold method was used to obtain the darker percentage of the picture which indicates the porosity (Ref 15).

Table 1 Plasma parameters during SolPS nanopowder synthesis

Plasma power	35 kW
Central gas (argon)	27 slpm
Sheath gas (oxygen)	80 slpm
Chamber pressure	13.3 kPa
Atomized gas flow rate (argon)	11.4 slpm

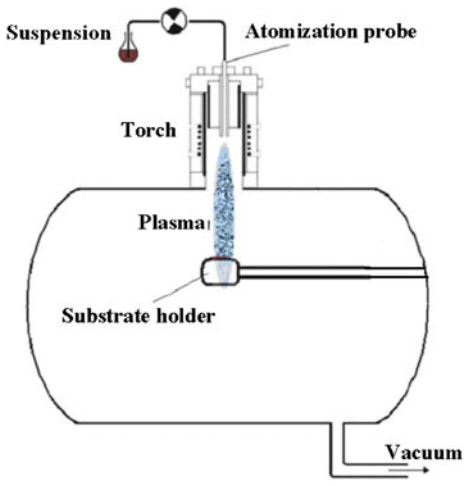

Fig. 2 Induction plasma deposition system

Table 2 Plasma parameters during SPS cathode deposition

Plasma power	35 kW
Central gas (argon)	27 slpm
Sheath gas (oxygen)	80 slpm
Chamber pressure	20.0 kPa
Spraying distance	220 mm
Atomized gas flow rate (argon)	11.4 slpm

3. Results and Discussions

3.1 SolPS Nanopowder

3.1.1 Morphologies of the Synthesized Powders. Figures 3 and 4 show the high resolution SEM pictures of the GDC6/LSCF4 and GDC3/LSCF7 nanocomposite powders collected from the filters, reactor and filter unit. From the SEM pictures, no significant morphology differences were found between the nanopowders collected from those three places. In order to get an evaluation of the morphology and the size of the nanopowder, TEM pictures of the two nanocomposite powders are presented in Fig. 5 and 6. All powders displayed in the pictures are almost globular in shape with nano-particle size mostly in the range of 10-60 nm and exhibiting no pronounced

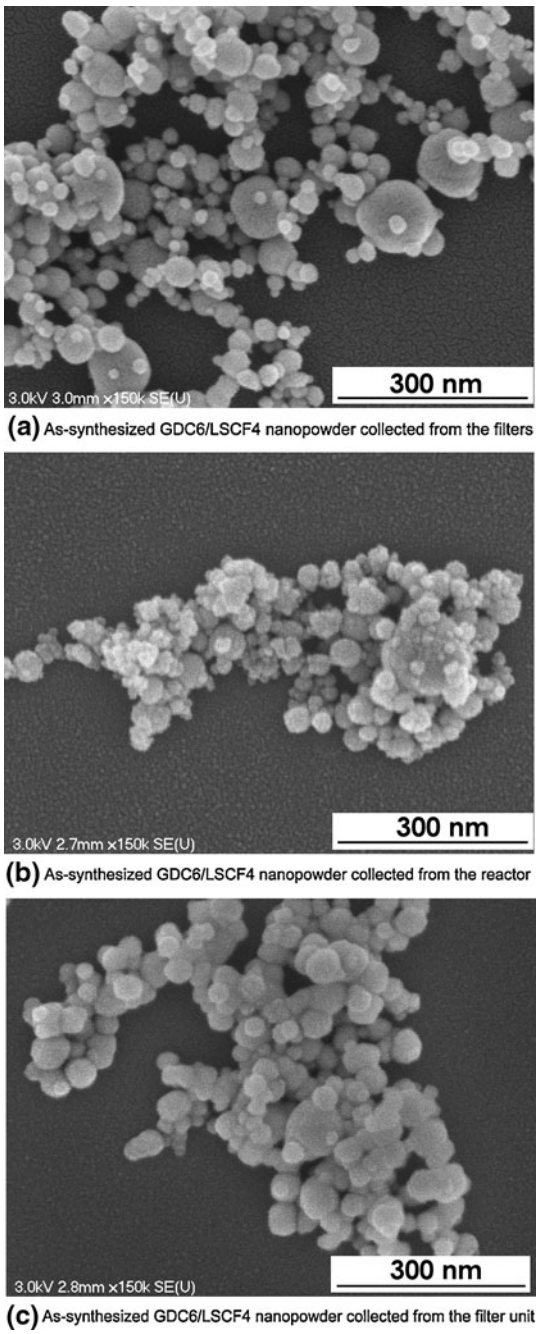

Fig. 3 SEM Micrograph of as-synthesized GDC6/LSCF4 nanopowder. (a) As-synthesized GDC6/LSCF4 nanopowder collected from the filters; (b) as-synthesized GDC6/LSCF4 nanopowder collected from the reactor; and (c) as-synthesized GDC6/LSCF4 nanopowder collected from the filter unit

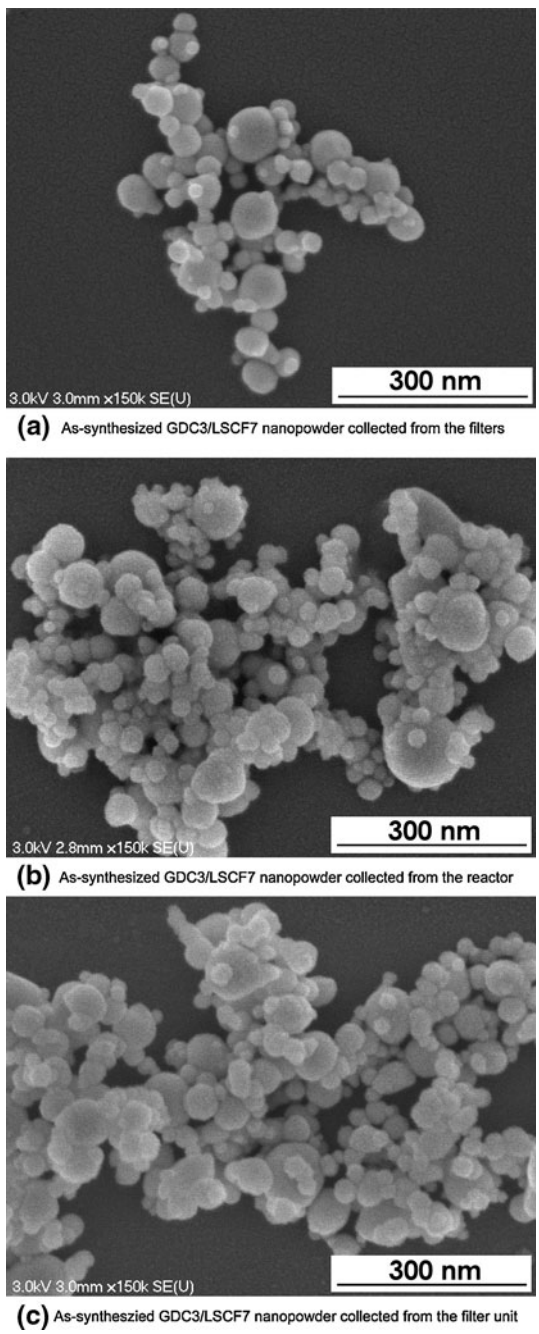

Fig. 4 SEM Micrograph of as-synthesized GDC3/LSCF7 nanopowder. (a) As-synthesized GDC3/LSCF7 nanopowder collected from the filters; (b) as-synthesized GDC3/LSCF7 nanopowder collected from the reactor; and (c) as-synthesziedGDC3/LSCF7 nanopowder collected from the filter unit

agglomeration. Preliminary tests with a 20 mL min^{-1} gave a stronger agglomeration as shown in Ref 6, so a reduced flow rate was applied in this study and resulted in less agglomeration of the nanoparticles.

Referring to the study of Bouchard and et al. (Ref 6), $La_{0.8}Sr_{0.2}MnO_3$, $La_{0.8}Sr_{0.2}FeO_3$ and $La_{0.8}Sr_{0.2}CoO_3$ nanopowders, synthesized under the same induction plasma conditions, had exactly the same particle size distribution, demonstrating that the particle size is independent of the composition. Based on their results, GDC nitrates were added into the LSCF nitrate solution, the concentrations of GDC nitrates were modified, and the injection flow rate was reduced from 20 to 5 mL min^{-1} after a preliminary test. The results show different concentrations of GDC metal nitrates in the precursor solution did not affect the size or the shape of the synthesized nanopowders. The synthesized GDC6/LSCF4 and GDC3/LSCF7 nanopowders show almost the same particle size ranges and shapes. The BET specific surface areas of as-synthesized GDC6/LSCF4 and GDC3/LSCF7 nanopowders are 20.8 and 19.6 m^2 g^{-1}, respectively. The similar BET specific surface areas demonstrate their close particle size distributions, since the density of these two nanopowders are similar, GDC6/LSCF4 (6.5 g cm^{-3}) and GDC3/LSCF7 (6.0 g cm^{-3}) as calculated using the mass ratio and the density of GDC (close to that of CeO_2: 7.13 g cm^{-3}) and LSCF (5.52 g cm^{-3}; Ref 16). Due to the low feeding rate, high plasma temperature and long residence time of the material in the plasma, it is reasonable that the variation between the metal nitrate precursor solutions of GDC6/LSCF4 and GDC3/LSCF7 did not have a strong influence on the thermal history in the plasma. Thus the morphologies of the final synthesized nanopowders are similar, as expected.

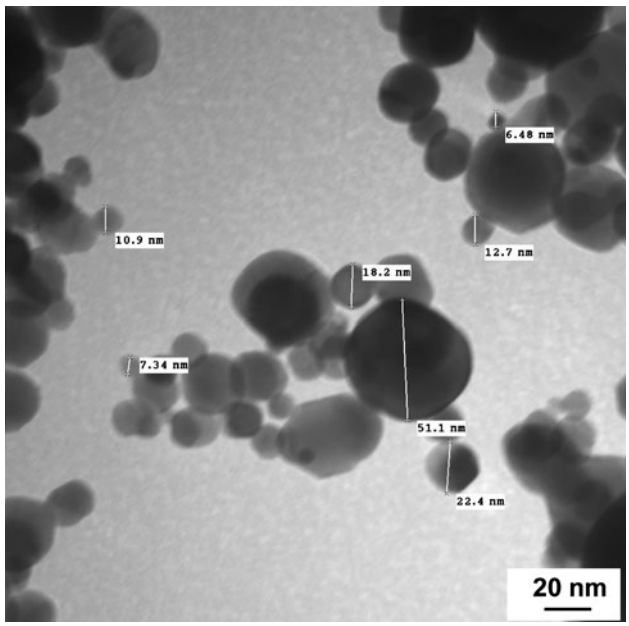

Fig. 5 TEM micrograph of as-synthesized GDC6/LSCF4 nanopowder collected from the filters

3.1.2 Composition and Phase Structure Study of the Synthesized Powders. It is not possible to identify the different phases of the nanoparticles from the normal TEM pictures, since all the particles in the pictures have almost the same darkness. Therefore, in order to get access to the local composition, EDS has been used in the Jeol TEM. Figures 7-10 show the results of local EDS phase analysis of the particles, with the EDS spectrums of

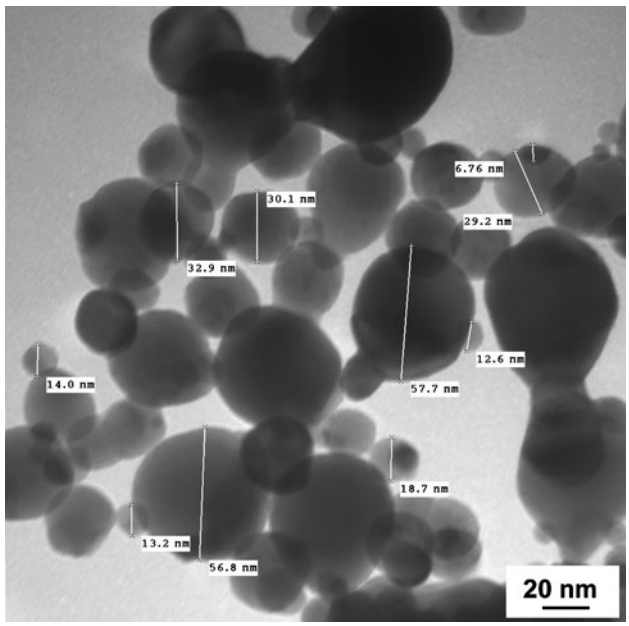

Fig. 6 TEM micrograph of as-synthesized GDC3/LSCF7 nanopowder collected from the filters

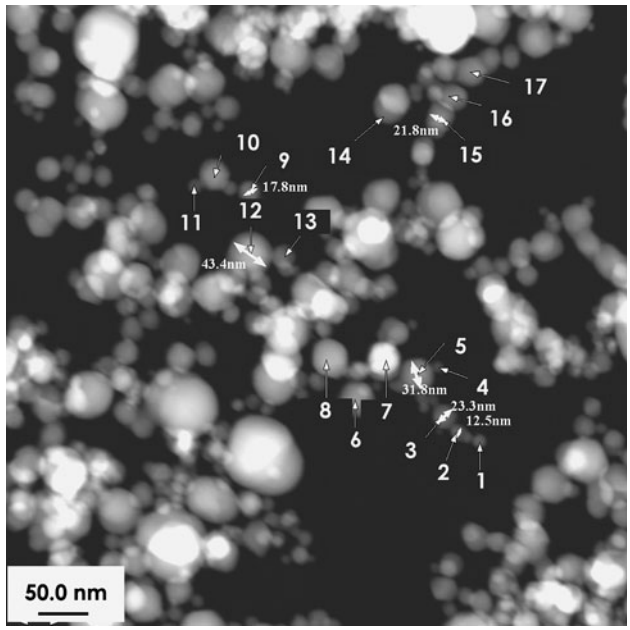

Fig. 7 TEM EDS local analysis figure of as-synthesized GDC6/LSCF4 nanopowder (refer to Table 3)

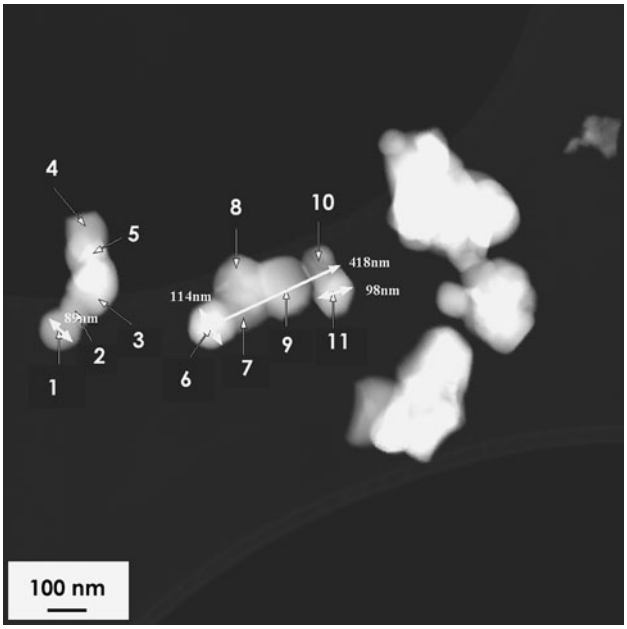

Fig. 8 TEM EDS local analysis figure of calcined GDC6/LSCF4 nanopowder (refer to Table 3)

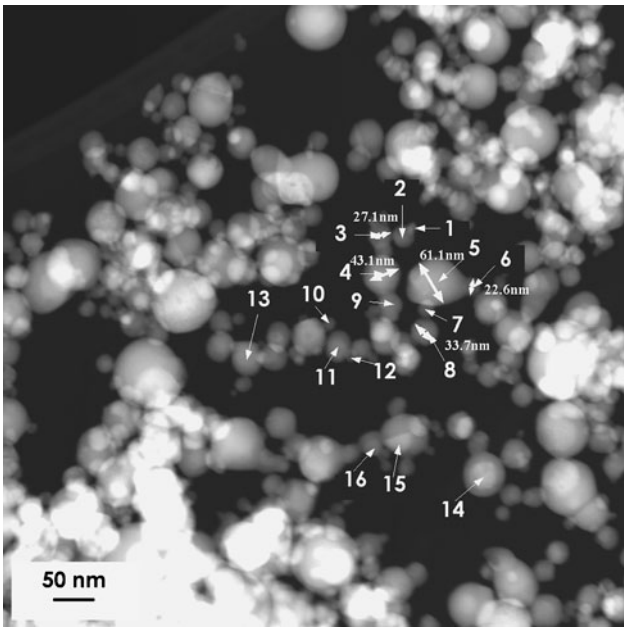

Fig. 9 TEM EDS local analysis figure of as-synthesized GDC3/LSCF7 nanopowder (refer to Table 3)

GDC, LSCF, and GDC/LSCF presented in Fig. 11 and Table 3. Separated GDC and LSCF phases can be identified from those pictures. However, some of the nanoparticles indicate the mixed phase of GDC/LSCF. Obviously, most of mixed compositions are the consequence of overlapping particles, such as the particles denoted with 7* in Fig. 7, 5* in Fig. 8, 11*, 14*, 15*, and 16* in Fig. 9, and 1*, 4*, and 5* in Fig. 10. Some of them show

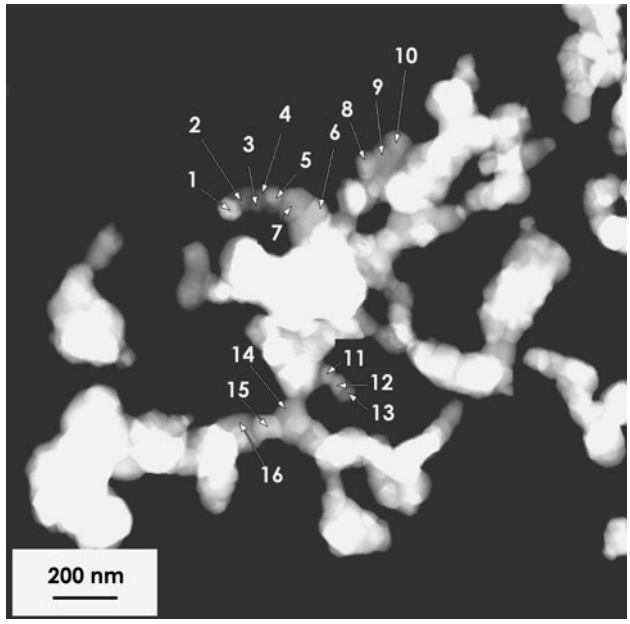

Fig. 10 TEM EDS local analysis figure of calcined GDC3/LSCF7 nanopowder (refer to Table 3)

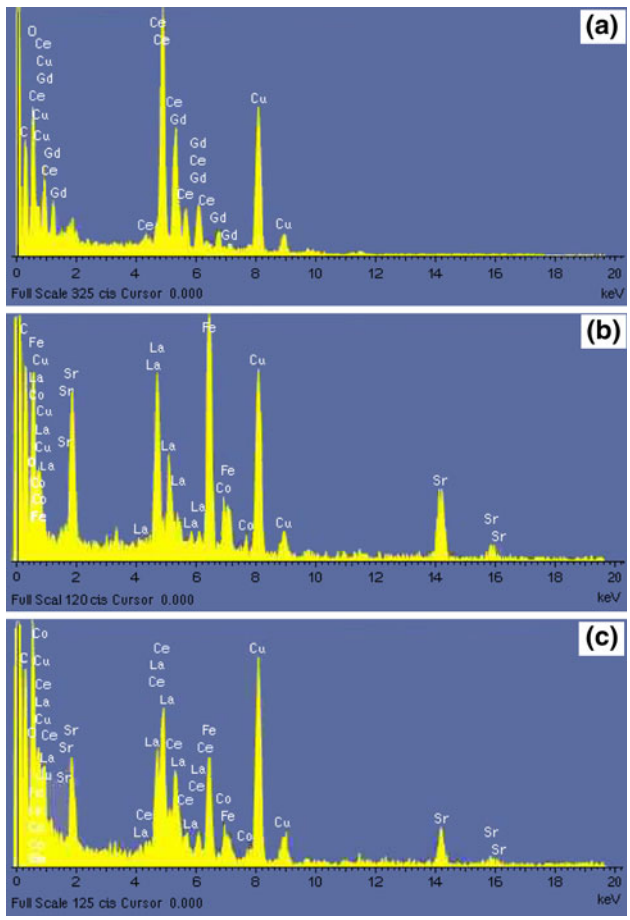

Fig. 11 EDS spectrum of the GDC (a), LSCF (b), and GDC/LSCF (c) phases (Cu is from the mesh for TEM characterization)

Table 3 EDS local composition analysis of synthesized nanopowders (Fig. 7-10)

	EDS label number			
Composition	**Figure 7**	**Figure 8**	**Figure 9**	**Figure 10**
GDC	3, 4, 5, 6, 9, 11, 15, 16	1, 2, 3, 4, 6, 8, 9, 10, 11	6, 12	6, 8, 10, 11, 12, 15
LSCF	2, 14, 17	7	1, 2, 5, 7, 8, 9	2, 3, 7, 9, 13, 14, 16
GDC/LSCF	1, 7*, 8, 10, 12, 13	5*	3, 4, 10, 11*, 13, 14*, 15*, 16*	1*, 4*, 5*

*Overlapping nanoparticles

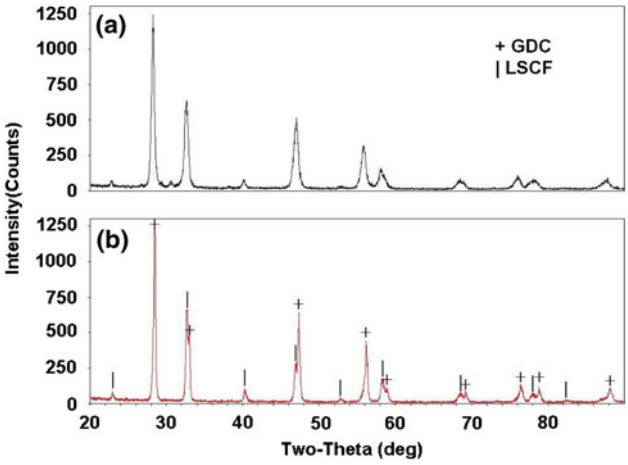

Fig. 12 XRD patterns of the nanocomposite powder GDC6/LSCF4 as-synthesized nanopowders (a) and calcined at 1000 °C for 2 h (b)

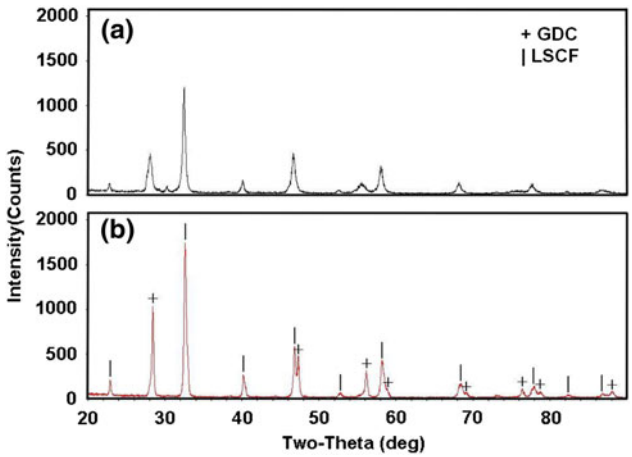

Fig. 13 XRD patterns of the nanocomposite powder GDC3/LSCF7 as-synthesized (a) and calcined at 1000 °C for 2 h (b)

distinguished brightness in the particle regions, and others show distorted spherical shapes. Eliminating the overlapping effect, the mixed phases of the particles are quite limited and almost disappeared in the nanopowders after calcinations. The phase segregation of the nanopowders becomes more obvious after the calcination. In addition, the LSCF and GDC phases are homogeneously distributed. This has the benefit of potentially increasing the TPB of the cathodes as the ion and electron conductors will be in close contact at the nanoscale.

The XRD diffraction patterns of these two mixed powders are presented in Fig. 12 and 13. Combining the results with local EDS analysis, the patterns before and after calcination exhibited mainly a perovskite structure of LSCF, according to the results of Leng et al. (Ref 5) and a fluorite structure of GDC. However, before the calcinations, limited quantities of undesired phases are revealed in the as-synthesized powders' patterns, which cannot be yet determined by using the existing 2004 spectra library JCPDS (ICDD, Newton Square, PA, USA). These are probably some metastable phases related to the mixed GDC/LSCF composition particles indicated in EDS analysis figures. They appear during plasma spray and are back to equilibrium after heat treatment. Moreover, some peaks of GDC are not quite distinguished from LSCF, especially in the nanopowder composite GDC3/LSCF7, because of the lower GDC concentration in the GDC3/LSCF7 powder. However, the powders after 2-h calcination at 1000 °C in air display a better crystallinity and only two pure phases are presented, indicating that the proper stoichiometric ratio of metal nitrates was added into the primary solution precursor as well as the absence of preferential evaporation of one of the elements.

By measuring the half-maximum width of the XRD line broadening, the average grain size can be estimated by the Scherrer equation. The grain sizes of LSCF and GDC are around 17 and 22 nm, respectively, in GDC6/LSCF4, and 21 and 14 nm in GDC3/LSCF7. All these results show the possibility to synthesize the nanocomposite powders of GDC/LSCF using induction plasma technology by a one-step solution spray process.

3.2 Coating Characteristics

3.2.1 Morphology and Microstructure of the Coating. As shown in Fig. 14, it was possible to successfully obtain a homogeneous and cauliflower-like structured cathode coating by the SPS induction plasma spray process with as-synthesized GDC6/LSCF4 nanopowder. Figure 14(a), which is a general surface of the cathode coating, shows that the micro-cauliflower particles have a diameter from 10 to 50 μm and are made of numbers of homogeneously distributed sub-micro or even nano-cauliflowers (Fig. 14b, c). The average open porosity is 51%, hence guaranteeing oxygen gas distribution. In addition, micron-size channels exist between the ''micro-cauliflower plants''

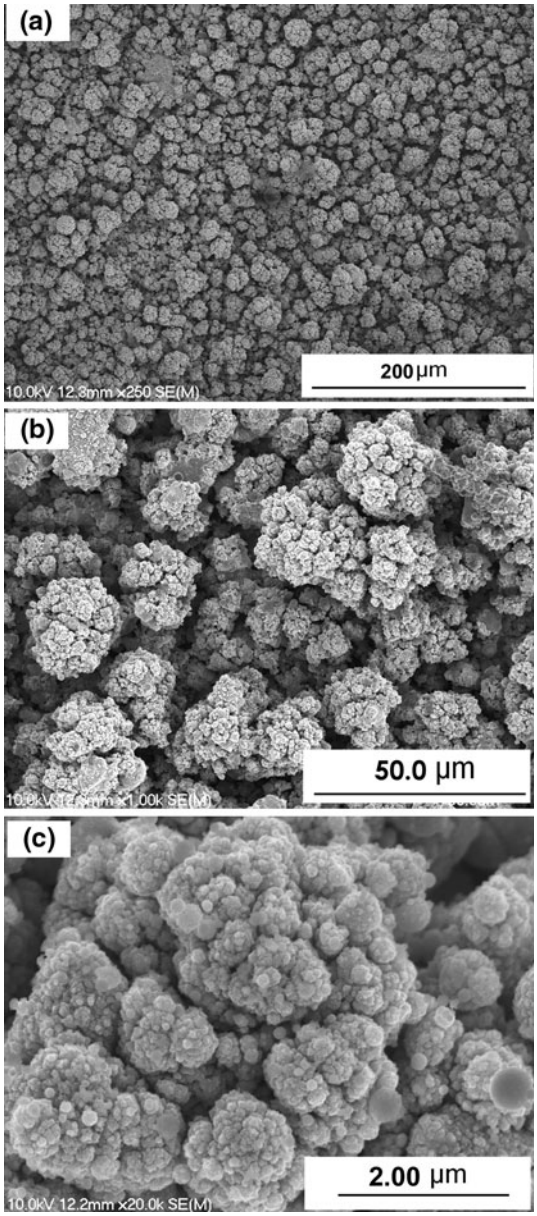

Fig. 14 SEM micrograph of the surface of SPS cathode coating (a) ×250, (b) ×1.00k, (c) ×20.0k magnification

(Fig. 15), facilitating the air and the oxygen-depleted air flow in the cathode. Because of the nano-cauliflower structures and the well-mixed ion and electron conductor phases, the TPBs are expected to be extended.

The contact between the SPS cathode coating and LSGFM electrolyte is excellent. No delaminations are found at the interface. That is because the nanocomposite particles are extremely well mixed, and so the thermal expansion coefficient (TEC) of the composite powders, between the high TEC of LSCF (17.5×10^{-6} K^{-1}; Ref 2) and low TEC of GDC (12.5×10^{-6} K^{-1}; Ref 16), is close to that of LSGFM (13.6×10^{-6} K^{-1}; Ref 17). Furthermore, the electrolyte, after the cathode deposition, is free from any cracks, showing the experiment parameters for

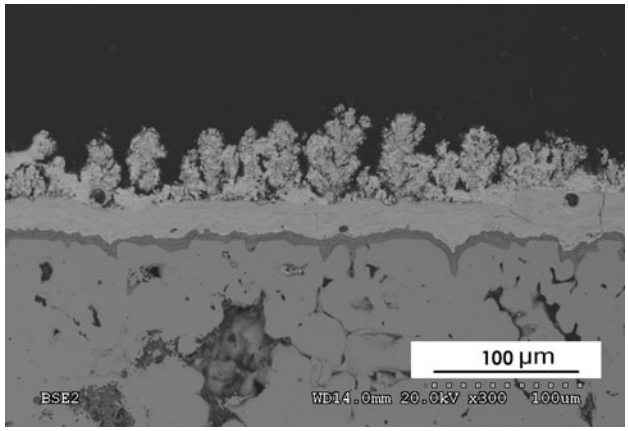

Fig. 15 SEM micrograph of the polished cross section of SPS cathode coating

the cathode deposition had no adverse influence on this electrolyte.

Moreover, using the SPS method, the thickness of the coating can be effectively controlled by altering the number of loops through the plasma plume. In this study, the 50-µm cathode coating has been built up in 2 min with a 30-loop deposition.

4. Conclusion and Future Work

Using induction plasma technology and SolPS, it is possible to achieve a homogeneously mixed nanosized composite GDC/LSCF powder without using a prolonged period of mechanical mixing. The nanopowders exhibit a perovskite structure and a fluorite structure as well as separated GDC and LSCF phases. Contamination of the powder can also be avoided, as the induction plasma technology has no electrodes. Moreover, by applying a low feeding rate, it is easy to synthesize nanopowders with different compositions by only adjusting the metal nitrate concentrations in the precursor solution. In addition, all the synthesized powders are spherical with a diameter between 10 and 60 nm regardless of their composition, demonstrating that the plasma parameter stability window is wide enough for the varied nanopowder synthesis.

A precursor suspension made with as-synthesized GDC6/LSCF4 powders and ethanol was used to deposit the cathode coating by SPS. The deposited coating had a homogeneous nano-cauliflower structure with an average porosity of 51%. It is expected to have lower polarization resistance as a result of enlarged TPBs due to the homogeneous nanoparticle distribution and fine coating microstructure. The optimized parameters for SPS cathode production have been preliminarily analyzed in this study. In the future, the cathode layer will be electrochemically characterized. The electrochemical tests will help us to confirm if there is a need for post-sintering of the coatings after plasma deposition. The electrochemical results of the SPS cathodes will also be compared with the SolPS

cathodes as well as with silk screened cathode using plasma synthesized nanopowder based pastes. In addition, GDC3/LSCF7 suspensions will be used with GDC6/LSCF4 suspensions to achieve nanostructured and graded composite cathode layer fabrication.

Acknowledgments

This research was partly supported through funding by the NSERC Solid Oxide Fuel Cell Canada Strategic Research Network from the Natural Science and Engineering Research Council (NSERC), and other sponsors listed at www.sofccanada.com. The authors would like to express their thanks to Hydro-Québec for the local EDS analysis, and to Mr. Daniel Calabretta, a Ph.D. student, for the provision of substrates for SPS GDC6/LSCF4 cathode deposition.

References

1. S.P. Jiang and J. Li, *Solid Oxide Fuell Cells: Materials Properties and Performance*, Chapter 3, CRC Press, 2009
2. A. Petric, P. Huang, and F. Tietz, Evaluation of La-Sr-Co-Fe-O Perovskites for Solid Oxide Fuel Cells and Gas Separation Membranes, *Solid State Ionics*, 2000, **135**(1-4), p 719-725
3. V. Dusastre and J.A. Kilner, Optimization of Composite Cathodes for Intermediate Temperature SOFC Applications, *Solid State Ionics*, 1999, **126**(1), p 163-174
4. E.P. Murray, M.J. Sever, and S.A. Barnett, Electrochemical Performance of (La, Sr)(Co, Fe)O_3-(Ce, Gd)O_2 Composite Cathodes, *Solid State Ionics*, 2002, **135**(1-2), p 27-34
5. Y. Leng, S.H. Chan, and Q. Liu, Development of LSCF-GDC Composite Cathodes for Low-Temperature Solid Oxide Fuel Cells with Thin Film GDC Electrolyte, *Int. J. Hydrogen Energy*, 2008, **33**(14), p 3808-3817
6. D. Bouchard, L. Sun, F. Gitzhofer, and G.M. Brisard, Synthesis and Characterization of $La_{0.8}Sr_{0.2}MO_{3-\delta}$ (M = Mn, Fe, or Co) Cathode Materials by Induction Plasma Technology, *J. Therm. Spray Technol.*, 2006, **15**(1), p 37-45
7. G. Schiller, M. Muller, and F. Gitzhofer, Preparation of Perovskite Powders and Coatings by Radio Frequency Suspension Plasma Spraying, *J. Therm. Spray Technol.*, 1999, **8**(3), p 389-392
8. F. Gitzhofer, E. Bouyer, and M.I. Boulos, Suspension Plasma Spraying, U.S. Patent No. 5,609,921, 1997
9. N.T. Hart, N.P. Brandon, M.J. Daya, and N. Lapena-Rey, Functionally Graded Composite Cathodes for Solid Oxide Fuel Cells, *J. Powder Sources*, 2002, **106**(1-2), p 42-50
10. S. Zha, Y. Zhang, and M. Liu, Functionally Graded Cathodes Fabricated by Sol-Gel/Slurry Coating for Honeycomb SOFCs, *Solid State Ionics*, 2005, **176**(1-2), p 25-31
11. P. Holtappels and C. Bagger, Fabrication and Performance of Advanced Multi-Layer SOFC Cathodes, *J. Eur. Ceram. Soc.*, 2002, **22**(1), p 41-48
12. A. Princivalle, D. Perednis, R. Neagu, and E. Djurado, Microstructural Investigations of Nanostructured La(Sr)$MnO_{3-\delta}$ Films Deposited by Electrostatic Spray Deposition, *Chem. Mater.*, 2004, **16**(19), p 3733-3739
13. Y. Liu, C. Compson, and M. Liu, Nanostructured and Functionally Graded Cathodes for Intermediate Temperature Solid Oxide Fuel Cells, *J. Power Sources*, 2004, **138**(1-2), p 194-198
14. M.I. Boulos, RF Induction Plasma Spraying: State-of-the-Art Review, *J. Therm. Spray Technol.*, 1992, **1**(1), p 33-40
15. M. von Bradke, F. Gitzhofer, and R. Henne, Porosity Determination of Ceramic Materials by Digital Image Analysis—A Critical Evaluation, *Scanning*, 2005, **27**(3), p 132-135
16. M. Mogensen, T. Lindegaard, and U.R. Hansen, Physical Properties of Mixed Conductor Solid Oxide Fuel Cell Anodes of CeO_2, *J. Electrochem. Soc.*, 1994, **141**(8), p 2122-2128
17. M. Enoki, J. Yan, H. Matsumoto, and T. Ishihara, High Oxide Ion Conductivity in Fe and Mg Doped $LaGaO_3$ as the Electrolyte of Solid Oxide Fuel Cells, *Solid State Ionics 15: Proceedings of the 15th International Conference on Solid State Ionics, Part I*, 2006, **177**(19-25), p 2053-2057